Hydrogel co-networks of gelatine methacrylate and poly(ethylene glycol) diacrylate sustain 3D functional *in vitro* models of intestinal mucosa

Anna Vila[1,#], Núria Torras[1,#], Albert G. Castaño[1], Maria García-Díaz[1], Jordi Comelles[1], Teresa Pérez-Berezo[1], Carmen Corregidor[1], Óscar Castaño[1,2,3], Elisabeth Engel[1,2,4], Vanesa Fernández-Majada[1,*], Elena Martínez[1,2,3,*]

[1]Institute for Bioengineering of Catalonia (IBEC), The Barcelona Institute of Science and Technology (BIST), c/Baldiri Reixac 10-12, 08028 Barcelona, Spain

[2]Centro de Investigación Biomédica en Red (CIBER), Av. Monforte de Lemos 3-5, Pabellon 11, Planta 0, 28029 Madrid, Spain

[3]Electronics and Biomedical engineering, University of Barcelona (UB), c/Martí i Franquès 1-11, 08028 Barcelona, Spain

[4]Materials Science and Metallurgical Engineering, Polytechnical University of Catalonia (UPC), c/Eduard Maristany 16, 08019 Barcelona, Spain

[#]equal contribution

[*]Corresponding authors: emartinez@ibecbarcelona.eu, vfernandez@ibecbarcelona.eu

Abstract

Mounting evidence supports the importance of the intestinal epithelial barrier and its permeability both in physiological and pathological conditions. Conventional *in vitro* models to evaluate intestinal permeability rely on the formation of tightly packed epithelial monolayers grown on hard substrates. These two-dimensional (2D) models lack the cellular and mechanical components of the non-epithelial compartment of the intestinal barrier, the stroma, which are key contributors to the barrier permeability *in vivo*. Thus, advanced *in vitro* models approaching the *in vivo* tissue composition are fundamental to improve precision in drug absorption predictions, to provide a better understanding of the intestinal biology, and to faithfully represent related diseases. Here, we generate photo-crosslinked gelatine methacrylate (GelMA) - poly(ethylene glycol) diacrylate (PEGDA) hydrogel co-networks that provide the required mechanical and biochemical features to mimic both the epithelial and stromal compartments of the intestinal mucosa, i.e., they are soft, cell adhesive and cell-laden friendly, and suitable for long-term culturing. We show that fibroblasts can be embedded in the GelMA-PEGDA hydrogels while epithelial cells can grow on top to form a mature epithelial monolayer that exhibits barrier properties which closely mimic those of the intestinal barrier *in vivo*, as shown by the physiologically relevant transepithelial electrical resistance (TEER) and permeability values. The presence of fibroblasts in the artificial stroma compartment accelerates the formation of the epithelial monolayer and boosts the recovery of the epithelial integrity upon temporary barrier disruption, demonstrating that our system is capable of successfully reproducing the interaction between different cellular compartments. As such, our hydrogel co-networks offer a technologically simple yet sophisticated approach to produce functional three-dimensional (3D) *in vitro* models of

epithelial barriers with epithelial and stromal cells arranged in a spatially relevant manner and near-physiological functionality.

Keywords: Gelatine methacrylate, poly(ethylene glycol) diacrylate, GelMA-PEGDA co-networks, intestinal mucosa, epithelial-stromal interactions, intestinal barrier function, intestinal permeability, hydrogels.

1. Introduction

The intestinal epithelium consists of a layer of tightly packed interconnected epithelial cells sitting on a collagen-based basal lamina that separates it from the stromal tissue (named *lamina propria*) below. The intestinal *lamina propria* contains many cell types including fibroblasts, myofibroblasts, endothelial and immune cells embedded in a matrix [1]. The intestinal epithelium in combination with the *lamina propria* form the intestinal mucosa, which functions as a pseudo-permeable barrier and ensures adequate containment of undesirable luminal contents while preserving the ability to absorb nutrients and beneficial substances [2]. It has been suggested that these barrier and permeability functions of the intestinal mucosa could play a crucial role in both physiological and pathological conditions [3]. For instance, intestinal drug permeability is a key parameter to take into account in the early stages of drug discovery [4,5]. At the same time, intestinal barrier dysfunction leading to increased intestinal permeability has been associated to numerous health conditions such as inflammatory bowel diseases, irritable bowel syndrome, celiac disease, obesity, and metabolic diseases [6]. Whether the inflammation associated with these diseases is a cause or a consequence of the increased intestinal permeability is still not fully understood [7]. Traditionally, intestinal permeability studies have been performed *in vivo* or using animal mucosal tissue explants. Although valuable, these experiments provide few mechanistic insights due to the complexity of the *in vivo* environment [8]. Conversely, *in vitro* models, which mostly use transformed epithelial cell lines grown as monolayers, provide a limited and simplistic representation of only the epithelial component of the intestinal mucosa. However, it has been demonstrated that epithelium-stroma interactions are important to maintain the intestinal mucosa integrity [9]. Thus, the development of more physiologically relevant 3D intestinal mucosa-like *in vitro* models that represent the epithelial and the stromal

compartments of the tissue in a spatially-relevant manner would be instrumental to narrow the gap between *in vitro* epithelial cell-based models and *in vivo* experiments.

Engineered tissues represent a new paradigm in the field of cell-based *in vitro* assays. They combine biofabrication and tissue-engineering components to provide *in vitro* models with tissue-like characteristics such as 3D architecture, multicellularity, cell-matrix interactions and near-*in vivo* functionality [10–13]. As such, engineered tissues hold the potential to deliver huge improvements over current reductionist cell culture monolayers, opening new research avenues by providing better tools for basic research, disease modelling, and drug testing. However, examples of engineered tissues recreating the intestinal mucosa and, more specifically, including stromal and epithelial components, are scarce. In a pioneering work, collagen hydrogels were used to embed primary mouse fibroblasts and produce a 3D model of the intestinal mucosa that included *lamina propria* and epithelial cells [14]. This models yielded improved predictions on drug permeability with respect to standard *in vitro* cultures based on tightly packed Caco-2 cell monolayers on Transwell®, which typically show abnormally high TEER values and low permeability values [14]. However, this model used fibroblasts with a low passage number to represent the stromal component, which compromises its adoption in routine long-term applications. A different study employed fibronectin-gelatine nanofilms to produce 3D-multilayer structures consisting of normal dermal fibroblast underneath a monolayer of epithelial Caco-2 cells [15]. The authors showed that the presence of multiple layers of dermal fibroblasts accelerates Caco-2 epithelial monolayer formation and enhances epithelial barrier function. In contrast, a more recent study showed how CCD-18Co intestinal fibroblasts embedded in Matrigel® were able to sustain the growth of epithelial cells, sitting on top of them, through the production of extracellular matrix proteins. The CCD-18Co fibroblasts interfered with barrier

robustness by getting intercalated between the epithelial cells [16]. The discrepancies reported with respect to the effects of stromal fibroblasts on the epithelial barrier performance is likely due to differences in experimental set-ups, particularly regarding the origin and density of the fibroblasts, the thickness of the construct, and the 3D organization of the epithelial and stromal compartments. As the literature in the field is sparse, further analysis of the impact of fibroblasts on the maintenance of the epithelial barrier maintenance is needed to elucidate the underlying mechanisms.

Thus far, most approaches to engineer 3D *in vitro* models of the intestinal mucosa that represent both the epithelial and stromal compartments, have employed hydrogels of natural origin as extracellular matrices (ECM). Typically, hydrogels are the preferred choice because they possess a high water content, mechanical properties that are similar to those in the native ECM of soft tissues, and confer diffusion-driven solute transport properties [17,18]. A major drawback of natural hydrogels is that they are highly biodegradable. On the one hand, this biodegradability allows for cell matrix remodelling, which can have positive effects on cell proliferation and migration [19,20]. However, on the other hand, it limits the time available for cell culturing and compromises the mechanical stability of the engineered tissues. Often, this problem is overcome by increasing the density of cells on the scaffold. However, this typically results in a density of cells that exceeds physiologically realistic levels in the native *lamina propria* and thus further removes these models from being able to faithfully represent *in-vivo* conditions [21].

In this work, we report a simple strategy to engineer a 3D model of the small intestinal mucosa that includes both the epithelium and the stroma components. To that aim, we employ hydrogels based on the co-polymerization of gelatine methacrylate (GelMA) and poly(ethylene glycol) diacrylate (PEGDA) polymers to produce cell-laden constructs.

GelMA provides cell-adhesive and biodegradable moieties, but its mechanical robustness is insufficient to sustain long-term cultures [17]. Conversely, PEGDA is a synthetic, non-degradable polymer that forms mechanically stable networks. We demonstrate that GelMA-PEGDA hydrogel co-networks generated by photopolymerization possess tuneable physicochemical and mechanical properties as a function of their polymer composition and total macromer content. For a particular co-network composition, we proved that fibroblasts-laden co-networks support the formation of a mature epithelial monolayer, providing an engineered *in vitro* model of the epithelial and stromal compartments. We then demonstrate that while our approach is sufficiently simple to be used with conventional cell culture systems, it also possesses the necessary complexity to recapitulate the relevant epithelial-stromal interactions, yielding realistic TEER values and an improved representation of the permeability of drug model compounds. The model can therefore be used to improve the predictive accuracy of state-of-the-art *in vitro* systems.

2. Materials and Methods

2.1. GelMA synthesis and characterization

Gelatine methacrylate (GelMA) was prepared following the method described previously [22,23] Briefly, a 10% (w/v) gelatine solution was obtained by dissolving gelatine from porcine skin type A (Sigma-Aldrich) in phosphate buffer saline (PBS; pH 7.4) (Gibco) at 50ºC under stirring conditions for approximately 2 h. Methacrylic anhydride (MA) (Sigma-Aldrich) at 5% v/v was added at a rate of 0.5 mL min^{-1} and left to react for 1 hour while stirring. Then, the solution was centrifuged at 1200 rpm for 3 min and the reaction was stopped by adding Milli-Q water to the supernatant. The resulting solution was dialyzed using 6-8 kDa MWCO membranes (Spectra/por, Spectrumlabs) against Milli-Q water at 40ºC, which was replaced every 4 h for 3 days. The pH of the dialyzed products

was adjusted to 7.4. Samples were frozen overnight at -80ºC and lyophilized for 4-5 days (Freeze Dryer Alpha 1-4 LD Christ). The resulting products were stored at -20ºC until further use.

The successful methacrylation of the synthesized GelMA was analysed by nuclear magnetic resonance (NMR) spectroscopy [24]. ^{1}H-NMR spectra were acquired using a Bruker DMX-500 high resolution NMR spectrometer (400 MHz) (Bruker). Spectra were collected from non-methacrylate gelatine as a control. To that end, GelMA solutions (1 mL) were prepared at 10 mg mL^{-1} in deuterium oxide. All spectra were collected with Mnova NMR software (Mestrelab Research). To quantitatively determine the amount of methacrylate amines in the GelMA polymer solutions, we employed the Habeeb Method [25]. This method is based on the fact that primary amines react with 2,4,6-Trinitrobenzene sulfonic acid (TNBS) (Sigma-Aldrich) to form a highly chromogenic derivative solution that can be measured by absorbance. Briefly, gelatine and GelMA polymers were dissolved at a concentration of 0.5 mg mL^{-1} in sodium bicarbonate buffer ($NaHCO_3$, 0.1M; pH 8.4, in Milli-Q water) (Sigma-Aldrich) at 40ºC under stirring conditions. To generate a standard curve, 100 µL of increasing concentrations of gelatine solution and 100 µL of GelMA solution at 0.5 mg mL^{-1} were placed in a 96 well plate. 50 µL of TNBS 0.01% solution in sodium bicarbonate buffer was added to each well and the mixture was incubated for 2 h at 37ºC in complete darkness. The TNBS reaction was stopped by adding 50 µL of sodium dodecyl sulfate 10% (SDS) (Sigma-Aldrich) and 25 µL of hydrochloric acid (HCl, 1M) (Panreac) to each well. The absorbance of the resulting solutions was measured at 335 nm using a spectrophotometer (Infinite M200 PRO Multimode Microplate Reader, Tecan). A linear calibration curve that relates the absorbances of the gelatine solution titrations to the free amine percentage (X) in the

sample was established. Then, the degree of methacrylation of the GelMA samples was calculated as: methacrylated amines (%) = 100 - X.

2.2. Fabrication of GelMA and GelMA-PEGDA hydrogels

GelMA polymer solutions containing two different concentrations of total macromers (7.5% and 12.5% w/v) were dissolved in DMEM without Phenol red (Gibco, Thermo Fisher Scientific) and complemented with 1% Penicillin-Streptomycin (Sigma-Aldrich) at 65ºC under stirring conditions. In addition, GelMA and PEGDA polymer solutions containing the same concentrations of total macromers (7.5% and 12.5% w/v) but different percentages of both polymers, namely 3.75% w/v GelMA- 3.75% w/v PEGDA and 7.5% w/v GelMA-5% w/v PEGDA, were prepared as follows. PEGDA, with a molecular weight of 4000 Da (Polysciences), was dissolved at 65ºC in DMEM without Phenol red (Gibco, Thermo Fisher Scientific) and complemented with 1% Penicillin-Streptomycin (Sigma-Aldrich) under stirring conditions for 2 h. Then, PEGDA solutions were filtered and mixed with the corresponding percentages of GelMA. Next, 2-Hydroxy-4′-(2-hydroxyethoxy)-2-methylpropiophenone photoinitiator (Irgacure D-2959) (Sigma-Aldrich) was added to the polymer solutions at a concentration of 0.5% w/v (Figure 1(a)). All polymer solutions were kept at 37ºC for about ~30 min before use. Hydrogel polymerization was performed following a previously described methodology [26] (Figure 1(b)). Briefly, an array of circular pools (6.5 or 10 mm in diameter) were produced by punching polydimethylsiloxane (PDMS) Sylgard 184 (Dow Corning) membranes (prepared at a ratio 10:1 w/w between the prepolymer and the curing agent and cured at room temperature for 24 h). The thickness of the hydrogel was defined by the height of the PDMS pools. Pools were mounted on top of polystyrene (PS) supports. Either silanized glass coverslips with a diameter of 12 mm or Tracketch® polyethylene terephthalate (PET) membranes with 5 µm pore size (Sabeu GmbH & Co) were then used

as substrates covering the tops of the PDMS pools. Polymer solutions were poured into the pool array and flood exposed to UV light to form disc-shaped hydrogels. UV light exposure took place in a MJBA mask aligner (SUSS MicroTech) equipped with an i-line filter (λ =365 nm) emitting an energy dose (power density x time) of 1.88 J cm^{-2}. Before each exposure, the incidental power density (power per surface unit) on the surface of the samples was measured using a UV-power meter (Model 1000, SUSS MicroTech) to properly adjust the exposure time. After UV exposure, unreacted polymer and photoinitiator were washed out with warmed PBS at 37ºC. Then, samples were kept submerged in PBS at 4ºC to reach equilibrium swelling before further characterization.

2.3. Characterization of GelMA and GelMA-PEGDA hydrogels

2.3.1 Analysis of co-network homogeneity. We determined the presence of GelMA and the microscopic homogeneity of the GelMA-PEGDA co-networks by the fluorescent labelling of the GelMA chains. For this purpose, discs of 10 mm in diameter and 1 mm in thickness, obtained by exposing to a UV dose of 3.00 J cm^{-2}, were fabricated onto glass coverslip substrates. Hydrogels were incubated overnight with a 0.02 mM solution of Rhodamine-NHS (Sigma-Aldrich) at 4ºC, which labels GelMA chains. After extensive washing in PBS, hydrogels were imaged using confocal microscopy (LSM 800, Zeiss). The average intensity was measured from the maximum Z projections of stacks of images collected from the first 50 µm of each hydrogel.

2.3.2 Mass swelling analysis. Hydrogel swelling was investigated on hydrogel discs (10 mm in diameter and 1 mm in height) photopolymerized with a UV dose of 1.88 J cm^{-2} onto glass coverslips covered with porous PET membranes (5 µm pore size). As PET membranes tend to absorb UV light [26], they were used during the characterization to have hydrogels with mechanical properties comparable to those employed in the cell

culture experiments. Right after polymerization, hydrogels were weighed (m_c) and kept submerged in PBS at 37ºC to induce swelling for one week, exchanging the PBS buffer every other day. Then, hydrogels were carefully wiped with a KimWipe (Kimtech Science) to remove any excess liquid and weighed again (m_s). Finally, samples were detached from the glass coverslips, frozen overnight at -80ºC, lyophilized (Freeze Dryer Alpha 1-4 LD Christ) and weighed once more (m_d). The mass swelling ratio for the GelMA and GelMA-PEGDA hydrogel co-networks was then calculated as the ratio between the mass due to swelling (difference between swollen and dry polymer) and the mass of the dry polymer.

$$Mass\ swelling\ ratio = \left(\frac{m_s - m_d}{m_d}\right).$$

2.3.3. Diffusion coefficient and mesh size analysis. Molecular diffusion is an important network property of the hydrogels affecting mass transport. To estimate the molecular diffusion in the GelMA samples, we used the Flory-Rehner theory [27] in its modified form by Peppas and Merrill [28]. The measured masses of the hydrogels right after fabrication (m_c), in equilibrium swelling (m_s), and in their dry state (m_d) were used to calculate the polymer volume fraction of the hydrogels in their swollen ($v_{2,s}$) and relaxed ($v_{2,r}$) states as well as their estimated mesh sizes ξ. Details of the calculation can be found in the Supplementary Information. Since this model is not well suited to determine the properties of hydrogel co-networks, we studied the influence of PEGDA within the GelMA networks by analysing the diffusion profiles of dextran fluorescent molecules of different molecular weights as they passed through the hydrogels. GelMA and GelMA-PEGDA hydrogel discs (6.5 mm in diameter and 1 mm in height) were fabricated on top of porous PET membranes (5 µm pore size) using a UV dose of 1.88 J cm^{-2}. Hydrogels were mounted on 24-well polycarbonate Transwell® filter inserts (Corning Costar) using

double-sided pressure-sensitive adhesive rings (Adhesives Research) as described elsewhere [26]. Then, 200 µL of solutions containing dextrans at 0.25 mg mL^{-1} in PBS were loaded in the apical chambers while adding 600 µL of PBS to the basolateral chambers. Dextran molecules of 4 kDa (FITC-Dextran), 70 kDa (Rhodamine-Dextran), and 500 kDa (FITC-Dextran) (all from Sigma-Aldrich) were used separately. The Transwell® plates were incubated at 37ºC. At regular intervals (from 0 to 240 min), 50 µL were sampled from the basolateral compartments and replaced with 50 µL of PBS. Collected samples were transferred to 96 black well plates and FITC or Rhodamine fluorescence was measured at excitation/emission wavelengths of 490/525 nm and 540/625 nm, respectively, using an Infinite M200 PRO Multimode microplate reader (Tecan). The changing concentration of dextrans over time was determined using standard calibration curves. Apparent diffusion coefficients (D_{app}) for each dextran were calculated as

$$D_{app} = \frac{P_{app} \cdot h}{K}$$

where *h* is the height of the hydrogels, *K* the hydrogel/water partition coefficient (assumed to be 1), and P_{app} the apparent permeability. P_{app} was obtained from the change in cumulative diffusion of the dextran over time (Figure S3) [29]. The effects of PEGDA on the network structure's mesh size were evaluated by comparing the apparent diffusion coefficients of the GelMA-PEGDA hydrogel co-networks to their GelMA counterparts (with equivalent macromer compositions).

2.4. Mechanical properties analysis

The mechanical properties of hydrogels are important physical cues that direct cell behaviour. For their measurement, we fabricated discs on top of coverslips covered with

a porous PET membrane. Pools, 10 mm in diameter and about 3 mm in height, were photopolymerized with an energy dose of 3.76 J cm^{-2} (double the standard dose to ensure photopolymerization across the entire thickness). After swelling in PBS, hydrogel diameters were no longer uniform and had to be re-punched to obtain consistent 10 mm diameter samples. Sample heights were accurately determined using a high precision Mitutoyo calliper (Mitutoyo Corporation). A Zwick-Roell Z0.5TN testing machine (Zwick Roell Group) was used to obtain stress-strain curves from compression assays at room temperature. Stress-strain curves were recorded limiting the strain rate to 5% min^{-1} and the maximum strain to 50%. An initial load of 5 mN was applied to facilitate proper contact between the hydrogels and the compression plates. The elastic modulus of the samples was determined using TestXpert II, v.3.41 analysis software to measure the slope of the linear region of the stress-strain curves, corresponding to a strain of 10-20%.

2.5. Degradation analysis

To investigate the degradation properties of GelMA and GelMA-PEGDA co-networks, we fabricated disc-shaped hydrogels (10 mm in diameter and 1 mm in thickness) on top of untreated cover glasses by applying a UV exposure dose of 3.00 J cm^{-2}. After fabrication, hydrogels were detached from the cover glasses and left to swell in an Eppendorf tube with 1 mL of PBS. After swelling, PBS was replaced by 1 mL of collagenase type II 2.5 U/mL solution (Sigma-Aldrich) and incubated at 37ºC for 96 hours while regularly removing collagenase solution by centrifuging the samples for 5 min at 8000 rpm. The undigested hydrogels were washed twice by adding Milli-Q water and centrifuged before decanting the supernatant. Then, the hydrogels were freeze-dried (Freeze Dryer Alpha 1-4 LD Christ) and weighed. The mass remaining percentage was determined by comparing the mass before (t=0) and after (t) enzyme incubation:

$$Mass\ remaning\ (\%) = \frac{M_{(t)}}{M_{(t=0)}} \cdot 100$$

2.6. Fabrication and characterization of cell-laden GelMA-PEGDA hydrogels

NIH-3T3 fibroblasts (ATCC® CRL-1658™) were used as cell model to mimic the stromal compartment of the intestinal tissue. Fibroblasts were expanded and maintained in 75 cm^2 flasks in high glucose DMEM (Gibco, Thermo Fisher Scientific), supplemented with 10% v/v fetal bovine serum (FBS) (Gibco, Thermo Fisher Scientific) and 1% v/v Penicillin/Streptomycin (Sigma-Aldrich). NIH-3T3 were grown in an incubator at 37ºC and 5% CO_2 (exchanging the medium every other day) and passaged twice a week. To produce cell-laden hydrogels, NIH-3T3 ($5 \cdot 10^6$ cells mL^{-1}) were trypsinised and re-suspended in pre-polymer solutions containing the polymers and 0.5% w/v Irgacure 2959 photoinitiator in DMEM supplemented with 1% v/v Penicillin/Streptomycin. DMEM without Phenol red was employed to avoid potential effects during photopolymerization. Cell-containing polymer solutions were kept at 37ºC before polymerization. Hydrogels (6.5 mm in diameter and 0.5 mm high) were fabricated on silanized PET membranes (5 µm pore size) (Figure 2(a)), by exposing them to a UV dose of 1.88 J cm^{-2}. Unreacted polymer and photoinitiator were washed out with warm cell culture medium supplemented with 10% of Penicillin/Streptomycin and 1/250 of normocin (Invitrogen). Cell-laden hydrogels were then attached to Transwell® inserts using PSA rings and cultured for 7 days in an incubator at 37ºC and 5% CO_2, exchanging the medium every other day. L-Ascorbic acid at 50 µg mL^{-1} (Sigma Aldrich) was added every other day to the cell culture medium to stimulate the production of extracellular matrix [30].

Cell viability on cell-laden hydrogels was investigated using a calcein-AM/ethidium homodimer Live/Dead kit (Invitrogen) 1 and 7 days after seeding and monitored via confocal laser scanning microscope (LSM 800, Zeiss). Image processing and cell viability

quantification was performed manually using ImageJ v.1.49b software (http://rsb.info.nih.gov/ij, NIH) to determine the percentage of viable cells at each time point.

2.7. Fabrication and functional characterization of a 3D model of the intestinal mucosa

2.7.1. Fabrication of the 3D model. Fibroblast-laden GelMA-PEGDA hydrogels were produced as described above to generate a model of the intestinal stromal compartment. Immediately after fabrication, Caco-2 cells (ATCC® HTB-37™) were seeded on top of the hydrogels to represent the epithelial component of the tissue. Caco-2 cells were maintained in 75 cm^2 flasks in high glucose DMEM (Gibco, Thermo Fisher Scientific), supplemented with 10% v/v fetal bovine serum (FBS) (Life Technologies), 1% v/v Penicillin/Streptomycin (Sigma Aldrich), and 1% v/v of non-essential amino acids (Gibco, Thermo Fisher Scientific). Cells were kept in an incubator at 37ºC and 5% CO_2 (exchanging the medium every other day) and passaged weekly. Caco-2 cells were seeded at a density of $7.5 \cdot 10^5$ cells cm^{-2} on the fibroblast-laden 7.5% w/v GelMA–5% w/v PEGDA hydrogel discs (6.5 mm in diameter, 0.5 mm high) fabricated onto PET porous membranes and mounted on Transwell® inserts. Control experiments were performed by seeding Caco-2 cells on fibroblast-free hydrogels of the same composition. Additionally, Caco-2 cells were seeded on standard 24-well polycarbonate Transwell® filter inserts (0.4 µm pore size) at a density of $7.5 \cdot 10^5$ cells cm^{-2}. Cells were cultured for 21 days, exchanging the medium every other day. The medium composition used for the co-culture was identical to the one used for the Caco-2 cells with the addition of L-ascorbic acid every other day.

2.7.2. Immunofluorescence and histological analysis. The characteristic morphology and polarization of Caco-2 cells forming an epithelial barrier were studied by immunostaining

after culturing for 21 days. Samples were fixed with 10% neutral buffered formalin solution (Sigma-Aldrich) at 4ºC for 1 hour, permeabilized with 0.5% Triton-X (Sigma-Aldrich) and blocked with 1% bovine serum albumin (Sigma-Aldrich), 3% donkey serum (Millipore), and 0.3% Triton-X. Primary antibodies against ZO-1 (Abcam) (2 µg mL^{-1}) and β-catenin (Abcam) (1 µg mL^{-1}) were incubated overnight at 4ºC under shacking conditions. Samples were then incubated with secondary antibodies and/or Rhodamine-Phalloidin (Cytoskeleton) (0.07 µM) for 2 h at 4ºC under shacking conditions. Anti-goat Alexa 488 (Invitrogen, Thermo Fisher Scientific) and anti-rabbit Alexa 647 (Invitrogen, Thermo Fisher Scientific) (4 µg mL^{-1}) were used as secondary antibodies. Finally, samples were incubated with DAPI (Thermo Fisher Scientific) (5 µg mL^{-1}) for 30 min.

For the hydrogel-embedded fibroblasts, cell morphology and extracellular matrix proteins production were analysed by immunofluorescence, following the same protocol described above. After fixation, permeabilization, and blocking steps, primary antibodies against Human Collagen IV (Biorad) (1.6 µg ml^{-1}) were incubated overnight at 4ºC under shacking conditions. Then, secondary antibodies anti-goat Alexa 488 (Invitrogen, Thermo Fisher Scientific) (4 µg mL^{-1}) and/or Rhodamine Phalloidin (Cytoskeleton) (0.07 µM) were incubated for 2 h at 4ºC under shacking conditions. Finally, samples were incubated with DAPI (5 µg mL^{-1}) for 30 min. After immunostaining, hydrogels were mounted facing downward onto glass coverslips and imaged using a confocal laser-scanning microscope (LSM 800, Zeiss). 500 µm PDMS spacers were employed to prevent sample damage. A drop of Fluoromount G (Southern Biotech) was added to preserve the dyes and prevent the sample from drying. Acquired Z-stacks were processed using Image J software. For a better visualization of the embedded cells across the entire height of the hydrogel, stained hydrogels were embedded and cross-sectioned using the optimal cutting temperature (OCT) technique. First, samples were incubated overnight with 30% sucrose

(Sigma-Aldrich) at 4ºC, then embedded in OCT (Tissue-Tek® O.C.T. Compound, Sakura® Finetek). OCT tissue sections (~7 μm in thickness) were cut, air dried, and stored at -80 C for further analysis. Alternatively, some samples were embedded in paraffin for later hematoxylin-eosin staining. These samples were embedded in an automatic tissue processor machine (Tissue Tek VIP, Sakura) following routine procedures and resulting in paraffin-embedded sections of about 3 μm thick. After being cut and air dried, these samples were further dried over-night at 60ºC and then stored at room temperature before hematoxylin and eosin staining. For later imaging, both types of hydrogel slices were mounted on a glass coverslip using Fluoromount G (Southern Biotech) and visualized using a confocal laser-scanning microscope (LSM 800, Zeiss).

2.7.3. Transepithelial electrical resistance and permeability studies. The integrity of the barrier developed by the epithelial cells on the fibroblast-laden hydrogels and control samples was monitored every two days throughout the culture period (21 days). For this purpose, the transepithelial resistance (TEER) between the two compartments of the Transwell® chambers was measured using an EVOM2 Epithelial voltohmmeter with an STX3 electrode (World precision Instruments). Measured resistance values were corrected by subtracting the resistances of the porous PET membranes and the hydrogels. TEER values were normalized to the total surface area of the epithelial monolayers. After 21 days, permeability was measured using FITC-dextrans of 4 kDa (FD4) as model compounds mimicking the paracellular transport of the epithelial layer through the tight junctions. In brief, cells were washed with DMEM without Phenol red (Gibco, Life Technologies) and 200 μL of the test compounds at a concentration of 0.5 mg mL^{-1} were added to the apical side of the Transwell® inserts. Then, 600 μL of DMEM without Phenol red were added to the basolateral compartments. Samples were collected from the

basolateral compartments at given time points followed by buffer replacement. During the experiment, cells were incubated at 37ºC on a horizontal shaker at 50 rpm. Samples were then placed into 96 black well plates and FITC fluorescence was measured using an Infinite M200 PRO Multimode microplate reader (Tecan) at 495/520 excitation/emission wavelengths. The apparent permeability (P_{app}) was determined from the change in cumulative diffusion of the dextran over time [29]. Finally, the impact of the stromal cells on barrier recovery after tight-junction disruption was studied after 21 days of culturing by disrupting the barrier with ethylenediaminetetraacetic acid (EDTA) (Sigma-Aldrich). 5 mM solution of EDTA in high glucose DMEM supplemented with 10% v/v fetal bovine serum (FBS), 1% v/v Penicillin/Streptomycin and 1% v/v of non-essential amino acids, were added to the apical (200 µL) and basolateral (600 µL) compartments. After 5 min of incubation, samples were washed with PBS and stored at 37ºC in DMEM, measuring TEER values at given time points.

2.8. Data analysis and statistics

The data are presented as the mean ± standard deviation (SD). The graphs were plotted using OriginPro 8.5 software (OriginLab). In the case of normal distributions, differences between groups were compared through a one-way analysis of variance (ANOVA). Turkey's test was performed as indicated in the figure legends. Differences were considered as statistically significant if $p < 0.05$.

3. Results

3.1. Photopolymerized GelMA and GelMA-PEGDA co-networks provide hydrogels with tuneable network properties

Nuclear magnetic resonance (NMR) spectroscopy of the methacrylation of the synthesized GelMA (Figure S1) yield bands at 5.3 ppm and the 5.6 ppm in the spectra of

the GelMA samples, characteristic of the double bonds of the methacrylate groups. Additionally, the decrease of a band at 3.0 ppm reveals the reaction of the methacrylic anhydride (MA) with the ε-amino groups from the Lysines in the gelatine [24]. These results confirm the success of the gelatine methacrylation process. By using the Habeeb Method [25], we found that adding 5% v/v of MA to the gelatine resulted in a polymer with a high degree of methacrylation (76.7 ± 2.1%). This parameter represents the percentage of ε-amino groups that are modified by the reaction, which determine the relative influence of the physical and chemical crosslinking mechanisms and, in turn, the mechanical properties of the final hydrogel [31]. As mechanical properties have been identified as critical cues affecting cellular behaviour [32], polymers with high degrees of methacrylation promoting chemical crosslinking are claimed to provide a more mechanically stable and cell-friendly environment [18].

GelMA, PEGDA and GelMA-PEGDA polymeric solutions were mixed with a photoinitiator (Irgacure 2959) placed in circular PDMS pools and crosslinked by UV, using exposure doses from 1 to 3.76 J cm^{-2} (Figure 1(a) and 1(b)) to form disc-shaped hydrogels. With this exposure conditions, only PEGDA polymers exhibited a complete lack of cross-linking at the macromer concentrations used. For all the solutions tested, UV dose of less than 1 J cm^{-2} lead to poorly crosslinked networks or no crosslinking at all.

GelMA has been shown to precipitate in GelMA-PEGDA co-networks when using high concentrations of PEG polymers of high molecular weight [33]. Through microscope imaging analysis of the distribution of fluorescence labelled GelMA chains we verified that GelMA precipitations did not occur in our composite hydrogel. We also did not observe any phase-segregation indicating the formation of homogeneous co-networks during the polymerization process (Figure S2).

The swelling properties of polymeric networks depend on both the pore size and the polymer-solvent interaction and are important as they can affect the diffusive and mechanical properties of the material [20,26,34]. In here, hydrogel swelling as a function of the total macromer concentration of the polymer (7.5% w/v or 12.5% w/v), showed that a higher macromer content led to significant decreases in swelling ratios for both the GelMA and GelMA-PEGDA samples (Figure 1(c)). This is a consequence of denser network structures that have higher crosslinking densities. In addition, the incorporation of PEGDA has a strong impact on the swelling properties of the co-network, increasing the hydrogels ability to attract and store water (Figure 1(c)). This effect, attributed to the higher hydrophilicity of the PEGDA polymeric chains, was more evident in samples with a lower macromer content (swelling ratio increased by 100% when adding PEGDA on 7.5% w/v samples and only by 54% when adding PEGDA on 12.5% w/v samples). This result is in agreement with previous findings [17].

Diffusivity analyses of dextran compounds of different molecular size were performed to gain insight on the porous nature of the hydrogels. Our results showed that the permeability of large to medium sized molecules such as FD500 and FD70 with molecular weights of 500 and 70 kDa and hydrodynamic diameters of 32 and 11.6 nm, respectively [35], were hindered by the hydrogels, while the smaller FD4 with 4 kDa of molecular weight and 2.8 nm of hydrodynamic diameter [36] could diffuse more easily (Figure S3). This effect was consistent for all the different hydrogels compositions (Figure 1(d)). For FD4, the diffusion coefficient decreased with increasing macromolecular content. This behaviour agrees with theoretical predictions of diffusivity for GelMA networks. We computed the values for the mesh size of PBS-swollen GelMA networks following Peppas and Merrill modifications proposed for the Flory-Rehner theory [27] (see supplementary Material and Methods), and found that those decreased from about 21 nm

to about 16 nm when the macromer content was increased from 7.5 to 12.5% w/v. PEGDA-containing hydrogels did not show significant differences in diffusivity properties with respect to their GelMA counterparts (Figure 1(d)), which suggests that mesh size is unaffected by the addition of PEGDA.

The mechanical properties of GelMA and GelMA-PEGDA hydrogels were evaluated in compression assays. The stress-strain curves recorded did not show any sample failure, even at the maximum strain level of 50%. This demonstrates that all hydrogels behaved as elastomers within the load range and the conditions of the assay. The bulk modulus significantly increased for higher macromer content, both in the GelMA and GelMA-PEGDA samples (Figure 1(e)), as would be expected for denser networks. For identical macromer contents, the addition of PEGDA led to a decrease in the bulk modulus, particularly (>90% decrease) for low (7.5% w/v) macromer content. The effects of adding PEGDA agree with those produced by a less dense network that allows higher water storage. Therefore, by co-polymerizing GelMA with PEGDA, the mechanical properties have become tuneable (here with bulk moduli ranging from 2 to 50 kPa) and comparable to those reported for soft tissues *in vivo* (1-100 kPa) [37].

We next investigated the effect of having GelMA-PEGDA co-networks on hydrogel degradation by incubating the different samples with collagenase. Our results showed that GelMA hydrogels containing 7.5% and 12.5% w/v of macromer were completely degraded after 4 and 24 hours, respectively (Figure 1(f)). This is in agreement with previous studies which showed that the crosslinking of GelMA macromers to form hydrogels did not interfere with their enzymatic degradability, and that the degradation rate rather depends on the amount of polymeric material [31]. We also found that for a given macromer content, the addition of PEGDA to form GelMA-PEGDA hydrogel co-networks retarded the degradation. Samples containing 7.5% w/v of GelMA and 5% w/v

of PEGDA were only 30% degraded after 96 h of collagenase incubation, preserving their mechanical integrity (Figure 1(f)). Any attempt to provide cells with artificial extracellular matrix (ECM) environments should synchronize the degradation rate needed for matrix remodelling with the rate of production of new ECM by the laden cells [17]. We found that GelMA-PEGDA hydrogels are able to modulate their degradation rates as the synthetic PEGDA component provides long-term mechanical integrity while the hydrogel-laden cells can attach, proliferate, and secrete their own ECM.

Overall, our GelMA-PEGDA co-networks are thus highly tuneable matrices in which water content, pore size, mechanical properties, and degradability can be tailored to suit the requirements of tissue-specific microenvironments.

3.2. GelMA-PEGDA hydrogel co-networks support fibroblast 3D culture

Based on the degradation results for the GelMA and GelMA-PEGDA samples and the long culture times required for the proper formation of intestinal epithelial cells (usually 3 weeks) [38], we selected the co-networks formed by 7.5% GelMA – 5% PEGDA for the cellular experiments. NIH-3T3 fibroblasts were mixed with the GelMA-PEGDA polymer solution and the photoinitiator before encapsulating them through exposure to a UV dose of 1.88 J cm^{-2} (Figure 2(a)). Disc-shaped hydrogels (6.5 mm in diameter and 0.5 mm thick) were initially loaded with $5 \cdot 10^6$ cells mL^{-1} cells. The hydrogel thickness was selected by considering that cell viability is limited by oxygen diffusion and computing the maximum hydrogel thickness for cell survival for NIH-3T3 cells (3 mm considering $2 \cdot 10^7$ cells mL^{-1}) [5]. The samples were fabricated on porous membranes and mounted on Transwell® inserts (Figure 2(a)). Cell viability of the encapsulated cells was evaluated through live/dead assays and confocal microscopy. One day after encapsulation, cells were evenly distributed throughout the hydrogel and, although there were some non-viable cells (stained in red), the majority were alive (stained in green) (Figure 2(b, c)).

Overall, cell viability, computed as the ratio between alive and dead cells, was greater than 85% right after encapsulation (Figure 2(d)). It has been previously shown that short-term cell viability after cell encapsulation is lost over time due to the stress induced by the photo-crosslinking process (UV irradiation, presence of radical species), and to the swelling caused by the incubation with cell culture medium. To evaluate these effects on our hydrogels, we analysed cell viability of the encapsulated cells at later culture time points. We found that at 7 days of culture, the cells were still evenly distributed along the thickness of the hydrogels (Figure 2(b), lower panel) and only a not statistically significant decrease of less than 10% in cell viability was observed (Figure 2(c), lower panel and Figure 2(d)). After 14 and 21 days of culture, cell viability had decreased considerably with most viable cells being located at or near the surface of the hydrogels (not shown). These results agree with previous findings where 3D environments have been reported to decrease cell metabolic activity and induce growth arrest, compared to 2D equivalents, leading to a metabolic steady state when cultured for long periods [16,39]. We next tested whether fibroblasts embedded in GelMA-PEGDA hydrogels were functional secreting ECM proteins. Specifically, we analysed the expression of collagen IV as relevant ECM protein of the stromal compartment and epithelial basement membrane. Immunostaining showed that embedded fibroblasts cultured for 7 days had spread thorough the hydrogel and were actively producing collagen IV (Figure 2(e)). In addition, embedded fibroblasts tested positive for the Ki67 proliferation marker after 7 days (Figure 2(e)). Fibroblasts that were growing closer to the surface of the hydrogel proliferated more and exhibit a broader spread morphology compared to cells located in the interior of the hydrogel (Figure 2(e), bottom panels). We hypothesize that these characteristics could be associated to hypoxic conditions and mass-transport issues inherent to the 3D cell culture microenvironment [37]. To test whether this limitation is

particular to our GelMA-PEGDA hydrogel co-network formulation or whether it might be overcome in future experiments, we conducted a pilot experiment with cell-laden hydrogels cultured in custom-made bioreactors, previously developed in our laboratory, with medium perfusion for 21 days [40]. We observed that the viable fibroblasts were homogenously distributed throughout the entire hydrogel when cultured in this bioreactor (Figure S4). However, for practical reasons, we chose to continue with the static Transwell® set-up in the work reported here.

Overall, our results show that GelMA-PEGDA co-networks guarantee a high level of viability and secretory functions of the encapsulated fibroblasts for at least 7 days in culture, making them convenient candidates for developing the stromal component of 3D *in vitro* models of intestinal mucosa.

3.3. GelMA-PEGDA hydrogel co-networks mimic the epithelial and stromal components of the intestinal mucosa

We next tested the capability of an epithelial intestinal cell line, Caco-2, to adhere and grow onto 7.5% GelMA - 5% PEGDA hydrogel co-networks. For this purpose, disc-shaped hydrogels 6.5 mm in diameter and 0.5 mm in height were photo-crosslinked by applying a UV exposure dose of 1.88 J/cm^2. The samples were fabricated onto porous polymeric membranes and mounted in Transwell® inserts. We next seeded $7.5 \cdot 10^5$ Caco-2 cells cm^{-2} onto the hydrogels and followed their behaviour throughout the culture. Our results show that Caco-2 cells were able to adhere, spread, and proliferate on the surface of our hydrogels. After 21 days of culture, confocal microscopy images revealed the formation of a densely packed monolayer of Caco-2 cells covering the entire surface of the hydrogel (Figure S5). Visualising β-catenin and ZO-1 markers via immunofluorescence reveal the typical cobblestone-like shape of epithelial layers (Figure 3(b), upper panels), while the cross-sections (Figure 3(b), lower panels) show columnar,

highly polarized cells exhibiting apical F-actin and ZO-1 expression, with β-catenin expression confined to the basolateral side of the monolayers. These results suggest that Caco-2 cells can form an epithelial monolayer on the GelMA-PEGDA hydrogel co-networks.

By combining the fibroblast-laden GelMA-PEGDA hydrogels with the culture of epithelial monolayers sitting on top of them we then obtained an *in vitro* model of the intestinal mucosa. NIH-3T3 cells were encapsulated at a density of $5 \cdot 10^6$ cells mL^{-1} following the method described in the previous section to generate fibroblasts-laden hydrogels that were mounted in Transwell® inserts and seeded with Caco-2 cells as described before (Figure 4(a)). After 21 days of culture, the hydrogels showed good mechanical integrity and could be processed to perform histological studies. Hematoxylin-eosin staining of the construct's cross-sections about 3 μm thick showed the formation of a continuous epithelial cell monolayer on top of the constructs and even distribution of fibroblasts throughout the hydrogel co-network (Figure 4(b)). Immunostaining showing apical F-actin and basolateral β-catenin confirmed the correct polarization of the epithelial monolayer formed on top of the mucosa-like hydrogel constructs. At this point in time, fibroblasts were mostly of a round shape while expressing collagen IV, which appears to have accumulated at the epithelial basement membrane (Figure 4(c)), suggesting their capacity to remodel the surrounding matrix. Based on these results, our GelMA-PEGDA hydrogel co-networks appear as excellent candidates to produce long-lasting *in vitro* models of the intestinal mucosa that would allow to mimic *in vivo* interactions between stromal and epithelial cells under physiological and pathological conditions.

3.4. *Evaluation of the stromal component effect on the barrier properties of the intestinal mucosa model*

As a proof of concept, we employed our 3D model of intestinal mucosa to assess *in vitro* the effect of fibroblasts on the intestinal epithelial monolayer growth and barrier function. As functional hallmarks for epithelial barrier integrity and permeability, we measured the transepithelial electrical resistance (TEER) and the apparent permeability (P_{app}) to paracellular model compounds of the epithelial monolayers grown under different experimental conditions. Hydrogel discs laden with fibroblasts were fabricated onto porous membranes, mounted on Transwell® inserts and seeded with Caco-2 cells following the methods earlier described. In addition, we used hydrogels discs without fibroblasts and seeded with Caco-2 cells, and Caco-2 cell monolayers grown directly on porous membranes, which is the current gold-standard culture format for these assays [41] (Figure 5(a)). Bright field images of the samples after 8 days of culture show that epithelial cells grown on fibroblast-laden hydrogels formed a continuous flat epithelial monolayer that fully covered the hydrogel surface. In contrast, on fibroblasts-free hydrogel samples the epithelial cells formed a discontinuous layer with dome-shaped structures (Figure 5(b)). TEER, which is directly related to the tightness of the epithelial barrier, increased in all samples including epithelial cells with increasing culture time (Figure 5(c)), indicating the formation of an epithelial monolayer with effective barrier properties. In contrast, fibroblast-laden hydrogels without epithelial cells on top (controls) did not show any significant change from the basal TEER background values (Figure S6), which conclusively demonstrates that the increase in TEER was due to the formation of an epithelial barrier. TEER values of Caco-2 epithelial monolayers grown on GelMA-PEGDA hydrogels were significantly lower (up to 4-fold) than for cells grown on hard Transwell® inserts (Figure 5(c)). It should be noted that TEER values of Caco-2 cell

monolayers grown on hard porous membranes increase already after 2-3 days in culture, while cells grown on GelMA-PEGDA hydrogels did not show an increase until 11-12 days of culture. This indicates a delay in epithelial layer formation when cells are gown on hydrogel substrates. It has been shown that the physical properties of cellular microenvironments play a crucial role in regulating cell division [42], collective cell migration [43], and, more importantly, in the maturing of tight junctions [44]. We therefore attribute the delay in epithelial monolayer formation and lower TEER values in the hydrogel-containing samples to the soft mechanical properties of the GelMA-PEGDA hydrogels (bulk modulus of about 35 kPa) compared to the Transwell® inserts (about 2 GPa). This is also in agreement with previous findings for soft natural [16,45] or synthetic hydrogels [26] which yield physiologically realistic values while hard porous membranes typically result in unrealistically high TEER values [46]. Hydrogel-based materials thus present near *in vivo*-like mechanical properties providing cells with an appropriate environment to grow and form epithelial monolayers that closely resemble the *in vivo* tissue barrier properties. Also, the change in TEER over time (slope) differed considerably between fibroblast-laden or fibroblasts-free GelMA-PEGDA hydrogels. The presence of fibroblasts clearly accelerated the monolayer formation and the development of tight junctions, which led to TEER values having increased 2.5-fold by day 21 (Figure 5(c)).

To further characterize the barriers, we investigated their permeability using FITC-dextran 4 kDa (FD4) as a tracer for paracellular transport through tight junctions. Consistent with the lower TEER values, the epithelial barriers formed onto the GelMA-PEGDA hydrogels were more permeable than those formed on Transwells® inserts (Figure 5(d)). Moreover, among the hydrogel samples, those containing embedded fibroblasts showed less epithelial permeability than those without fibroblasts (Figure

5(d)). These results indicate that the presence of embedded fibroblasts in the hydrogel had a positive effect on the formation of a continuous and uniform epithelial monolayer with mature tight junctions that lead to higher TEER and lower permeability than in epithelial monolayer formed on hydrogels devoid of fibroblasts.

3.5. Effects of stromal components on the recovery of the barrier function of the intestinal epithelium

We used our *in vitro* model of the intestinal mucosa to mimic the loss of epithelial barrier integrity, a common occurrence under specific pathological conditions. Epithelial monolayers grown on fibroblast-laden or fibroblast-free GelMA-PEGDA hydrogels were grown for 21 days as previously described, and then treated shortly with EDTA to disrupt the tight junctions and increase permeability. Epithelial integrity was monitored by measuring TEER values at different time points from the moment we added the EDTA to 24 hours after removing it. As expected, treatment with EDTA reduced the TEER values in both samples to basal levels (Figure 5(e)). After removing EDTA, TEER values recovered due to the recovery of the tight junctions and associated barrier integrity of the epithelial monolayers. Interestingly, TEER recovered more quickly in epithelial monolayers grown on fibroblast-laden hydrogels than in those formed on fibroblast-free hydrogels (Figure 5(e, f)). These results indicate that the presence of stromal fibroblasts not only affects the Caco-2 monolayer growth rate, morphology, and permeability, but also the rate of recovery of a barrier following a temporary disruption of the tight junctions.

4. Discussion

Intestinal epithelial-stromal interactions play an important role in regulating fundamental biological processes both under physiological and pathological conditions [9,21,47,48]. It is therefore crucial to engineer more physiologically relevant *in vitro* models of intestinal mucosa that represent not only the epithelial but also the cellular and matrix components of the stroma. Despite recent advances, the set-ups are often highly complex which limits their use in routine assays [49, 15]. Furthermore, most studies employed biodegradable hydrogels of natural origins [14,16], which greatly compromises the mechanical stability of the constructs over time and, thus, their life span.

Here we have presented a simple procedure to fabricate a co-network formed by gelatine methacrylate (GelMA), a natural-derived polymer, and poly(ethylene glycol) diacrylate (PEGDA), a synthetic polymer, to produce a mechanically stable and long-lasting 3D model of the intestinal mucosa. The covalently crosslinked GelMA-PEGDA co-networks possess adjustable swelling, mesh size, degradability, and mechanical properties, resulting in a versatile system that can emulate the physicochemical properties of tissue extracellular matrices, which combine rigid and soft networks to provide mechanical stability, cell-adhesion properties, and matrix remodelling capabilities [17,49]. We demonstrated that GelMA-PEGDA hydrogel co-networks can sustain viable and functional embedded fibroblasts that emulate the cellular component of the stromal compartment of the intestinal mucosa. In addition, we could show that epithelial cell monolayers can be successfully grown on top of the fibroblast-laden hydrogels. After 21 days in culture, epithelial monolayers formed on GelMA-PEGDA co-networks were nicely polarized and expressed typical epithelial markers. The effective tissue barrier function of the epithelial monolayers was evaluated by TEER and permeability measurements. We found that both were significantly increased when fibroblasts were embedded in the hydrogels. Using a model of pathological intestinal barrier disruption,

we showed that the presence of fibroblasts in the artificial stroma accelerated the recovery of the tight junctions and the barrier function of the damaged epithelium returning them to physiological levels. Remarkably, the effects of the NIH-3T3 fibroblasts on the Caco-2 epithelial cells were noticeable despite using fibroblasts of a murine non-intestinal origin at low densities. NIH-3T3 fibroblasts have been extensively used in co-cultures with murine but also with human cells as feeder layers [50]. While it is well known that NIH-3T3 favours cell growth through paracrine signalling, the underlying mechanisms are still not fully understood. Co-cultures of fibroblasts and Caco-2 epithelial cells in conventional Transwell® inserts have been reported to enhance epithelial proliferation and differentiation via paracrine effects of the fibroblasts such as hepatocyte growth factor (HGF) [47] or keratinocyte growth factor (KGF) [51]. No tissue specificity for the fibroblast action was detected in these studies. In addition, mesenchymal-stromal cells have also been reported to accelerate tight junction assembly in epithelial monolayers [44]. Paracrine signalling also seems to be the main signalling source of NIH-3T3 fibroblasts in our mucosa model, as their growth appeared inhibited and we did not see any physical interaction between them and the epithelial cells.

Overall, our results demonstrate that GelMA-PEGDA hydrogel co-networks might be good candidates to produce long-lasting *in vitro* models of the intestinal mucosa with the epithelial and mesenchymal compartment being represented in a cell-spatial configuration recapitulating the one found *in vivo*. Combining natural and synthetic polymers to generate the scaffold we could ensure both the integrity of the construct for long periods of time (at least 21 days of culture) and the compatibility with cell growth and functionality of the embedded cells. Furthermore, we showed that embedded fibroblasts do express collagen IV which indicates their capacity to remodel the surrounding matrix by creating new matrix or by degrading the existing one [16]. Thus,

our PEGDA-GelMA hydrogel co-networks would allow to mimic *in vivo* interactions between mesenchymal and epithelial cells that would help us understanding better biological processes that depend on cell migration, cell-cell interactions and cell-matrix interactions, both under physiological and pathological conditions.

5. Conclusion

Our intestinal mucosa model based on GelMA-PEGDA hydrogel co-networks was able to mimic some of the features attributed to mesenchymal-epithelial interactions such as enhanced epithelial cell proliferation and barrier permeability, diffusivity properties that allow paracrine effects and accelerated tight junction recovery. As added benefits, our 3D model possesses a tissue-like architecture that includes both stromal and epithelial compartments arranged in a spatially relevant manner as well as *in vivo*-like mechanical properties of the substrate. This enables to model cell-to-cell and cell-to-matrix interactions with *in vivo*-like accuracy, which translates into more physiological values of intestinal permeability hallmarks (TEER and permeability). Our model provides a simplistic but still meaningful approach to obtain more physiologically relevant *in vitro* epithelial models at the cellular and functional levels. It can therefore be used to improve predictions of intestinal permeability in drug studies or to implement better epithelial disease models where an accurate reproduction of the interaction between different cell compartments is of crucial importance. These GelMA-PEGDA co-networks should be able to accommodate additional relevant stromal cellular components such as the immune system (pivotal for regulating inflammatory responses, metabolic and cancerogenic processes) while being sufficiently versatile to mimic other simple or stratified epithelial tissues such as oesophagus, stomach, or skin.

Acknowledgements

Funding for this project was provided by a European Union Horizon 2020 ERC grant (agreement no. 647863 - COMIET), the CERCA Programme/Generalitat de Catalunya (2017-SGR-1079), and the Spanish Ministry of Economy and Competitiveness (TEC2014-51940-C2-2-R, TEC2017-83716-C2-1-R, and the Severo Ochoa Programme for Centres of Excellence in R&D 2016-2019). M. G.-D. would like to acknowledge financial support through the BEST Postdoctoral Programme, funded by the European Commission under the Horizon 2020 Marie Skłodowska-Curie Actions COFUND scheme (grant agreement no. 712754) and by the Severo Ochoa programme of the Spanish Ministry of Science and Competitiveness (Grant SEV-2014-0425, 2015-2019). The collaboration of the MicroFabSpace from IBEC is gratefully acknowledged. The results presented here only reflect the views of the authors; the European Commission is not responsible for any use that may be made of the information it contains.

References

1. Hunyady, B.; Mezey, E.; Palkovits, M. Gastrointestinal immunology: cell types in the lamina propria--a morphological review. *Acta Physiol. Hung.* **2000**, *87*, 305–28.
2. Turner, J.R. Intestinal mucosal barrier function in health and disease. *Nat. Rev. Immunol.* **2009**, *9*, 799–809.
3. Vancamelbeke, M.; Vermeire, S. The intestinal barrier: a fundamental role in health and disease. *Expert Rev. Gastroenterol. Hepatol.* **2017**, *11*, 821–834.
4. Artursson, P.; Karlsson, J. Correlation between oral drug absorption in humans and apparent drug permeability coefficients in human intestinal epithelial (Caco-2) cells. *Biochem. Biophys. Res. Commun.* **1991**, *175*, 880–5.
5. Yanagawa, F.; Kaji, H.; Jang, Y.-H.; Bae, H.; Yanan, D.; Fukuda, J.; Qi, H.;

Khademhosseini, A. Directed assembly of cell-laden microgels for building porous three-dimensional tissue constructs. *J. Biomed. Mater. Res. A* **2011**, *97*, 93–102.

6. Bischoff, S.C.; Barbara, G.; Buurman, W.; Ockhuizen, T.; Schulzke, J.-D.; Serino, M.; Tilg, H.; Watson, A.; Wells, J.M. Intestinal permeability--a new target for disease prevention and therapy. *BMC Gastroenterol.* **2014**, *14*, 189.
7. Wang, K.; Wu, L.-Y.; Dou, C.-Z.; Guan, X.; Wu, H.-G.; Liu, H.-R. Research Advance in Intestinal Mucosal Barrier and Pathogenesis of Crohn's Disease. *Gastroenterol. Res. Pract.* **2016**, *2016*, 9686238.
8. Maresca, M.; Pinton, P.; Ajandouz, E.H.; Menard, S.; Ferrier, L.; Oswald, I.P. Overview and Comparison of Intestinal Organotypic Models, Intestinal Cells, and Intestinal Explants Used for Toxicity Studies. *Curr. Top. Microbiol. Immunol.* **2018**, 1–18.
9. Bosman, F.T.; de Bruïne, A.; Flohil, C.; van der Wurff, A.; ten Kate, J.; Dinjens, W.W. Epithelial-stromal interactions in colon cancer. *Int. J. Dev. Biol.* **1993**, *37*, 203–11.
10. Martínez, E.; St-Pierre, JP.; Variola, F. Advanced bioengineering technologies for preclinical research. *Adv. Phys. X* **2019**, *4*, 1–28.
11. Torras, N.; García-Díaz, M.; Fernández-Majada, V.; Martínez, E. Mimicking Epithelial Tissues in Three-Dimensional Cell Culture Models. *Front. Bioeng. Biotechnol.* **2018**, *6*, 197.
12. Duval, K.; Grover, H.; Han, L.-H.; Mou, Y.; Pegoraro, A.F.; Fredberg, J.; Chen, Z. Modeling Physiological Events in 2D vs. 3D Cell Culture. *Physiology (Bethesda).* **2017**, *32*, 266–277.
13. Turnbull, I.C.; Karakikes, I.; Serrao, G.W.; Backeris, P.; Lee, J.-J.; Xie, C.;

Senyei, G.; Gordon, R.E.; Li, R.A.; Akar, F.G.; et al. Advancing functional engineered cardiac tissues toward a preclinical model of human myocardium. *FASEB J. Off. Publ. Fed. Am. Soc. Exp. Biol.* **2014**, *28*, 644–654.

14. Li, N.; Wang, D.; Sui, Z.; Qi, X.; Ji, L.; Wang, X.; Yang, L. Development of an improved three-dimensional in vitro intestinal mucosa model for drug absorption evaluation. *Tissue Eng. Part C. Methods* **2013**, *19*, 708–19.
15. Matsusaki, M.; Hikimoto, D.; Nishiguchi, A.; Kadowaki, K.; Ohura, K.; Imai, T.; Akashi, M. 3D-fibroblast tissues constructed by a cell-coat technology enhance tight-junction formation of human colon epithelial cells. *Biochem. Biophys. Res. Commun.* **2015**, *457*, 363–9.
16. Pereira, C.; Araújo, F.; Barrias, C.C.; Granja, P.L.; Sarmento, B. Dissecting stromal-epithelial interactions in a 3D in vitro cellularized intestinal model for permeability studies. *Biomaterials* **2015**, *56*, 36–45.
17. Daniele, M.A.; Adams, A.A.; Naciri, J.; North, S.H.; Ligler, F.S. Interpenetrating networks based on gelatin methacrylamide and PEG formed using concurrent thiol click chemistries for hydrogel tissue engineering scaffolds. *Biomaterials* **2014**, *35*, 1845–56.
18. Fu, Y.; Xu, K.; Zheng, X.; Giacomin, A.J.; Mix, A.W.; Kao, W.J. 3D cell entrapment in crosslinked thiolated gelatin-poly(ethylene glycol) diacrylate hydrogels. *Biomaterials* **2012**, *33*, 48–58.
19. Aubin, H.; Nichol, J.W.; Hutson, C.B.; Bae, H.; Sieminski, A.L.; Cropek, D.M.; Akhyari, P.; Khademhosseini, A. Directed 3D cell alignment and elongation in microengineered hydrogels. *Biomaterials* **2010**, *31*, 6941–6951.
20. Nichol, J.W.; Koshy, S.T.; Bae, H.; Hwang, C.M.; Yamanlar, S.; Khademhosseini, A. Cell-laden microengineered gelatin methacrylate hydrogels.

Biomaterials **2010**, *31*, 5536–5544.

21. Powell, D.W.; Pinchuk, I. V; Saada, J.I.; Chen, X.; Mifflin, R.C. Mesenchymal cells of the intestinal lamina propria. *Annu. Rev. Physiol.* **2011**, *73*, 213–37.
22. Van Den Bulcke, A.I.; Bogdanov, B.; De Rooze, N.; Schacht, E.H.; Cornelissen, M.; Berghmans, H. Structural and rheological properties of methacrylamide modified gelatin hydrogels. *Biomacromolecules* **2000**, *1*, 31–8.
23. Loessner, D.; Meinert, C.; Kaemmerer, E.; Martine, L.C.; Yue, K.; Levett, P.A.; Klein, T.J.; Melchels, F.P.W.; Khademhosseini, A.; Hutmacher, D.W. Functionalization, preparation and use of cell-laden gelatin methacryloyl-based hydrogels as modular tissue culture platforms. *Nat. Protoc.* **2016**, *11*, 727–46.
24. Li, X.; Chen, S.; Li, J.; Wang, X.; Zhang, J.; Kawazoe, N.; Chen, G. 3D Culture of Chondrocytes in Gelatin Hydrogels with Different Stiffness. *Polymers (Basel).* **2016**, *8*.
25. Habeeb, A.F.S.A. Determination of free amino groups in proteins by trinitrobenzenesulfonic acid. *Anal. Biochem.* **1966**, *14*, 328–336.
26. Castaño, A.G.; García-Díaz, M.; Torras, N.; Altay, G.; Comelles, J.; Martínez, E. Dynamic photopolymerization produces complex microstructures on hydrogels in a moldless approach to generate a 3D intestinal tissue model. *Biofabrication* **2019**, *11*, 025007.
27. Flory, P.J.; Rehner, J. Statistical Mechanics of Cross-Linked Polymer Networks I. Rubberlike Elasticity. *J. Chem. Phys.* **1943**, *11*, 512–520.
28. Peppas, N.A.; Merrill, E.W. Crosslinked poly(vinyl alcohol) hydrogels as swollen elastic networks. *J. Appl. Polym. Sci.* **1977**, *21*, 1763–1770.
29. Kontturi, L.-S.; Collin, E.C.; Murtomäki, L.; Pandit, A.S.; Yliperttula, M.; Urtti, A. Encapsulated cells for long-term secretion of soluble VEGF receptor 1:

Material optimization and simulation of ocular drug response. *Eur. J. Pharm. Biopharm.* **2015**, *95*, 387–97.

30. Caballero, D.; Samitier, J. Topological control of extracellular matrix growth: A native-like model for cell morphodynamics studies. *ACS Appl. Mater. Interfaces* **2017**, *9*, 4159–4170.
31. Benton, J.A.; DeForest, C.A.; Vivekanandan, V.; Anseth, K.S. Photocrosslinking of gelatin macromers to synthesize porous hydrogels that promote valvular interstitial cell function. *Tissue Eng. Part A* **2009**, *15*, 3221–30.
32. Engler, A.J.; Sen, S.; Sweeney, H.L.; Discher, D.E. Matrix elasticity directs stem cell lineage specification. *Cell* **2006**, *126*, 677–89.
33. Hönig, W.; Kula, M.R. Selectivity of protein precipitation with polyethylene glycol fractions of various molecular weights. *Anal. Biochem.* **1976**, *72*, 502–12.
34. Peppas, N.A.; Hilt, J.Z.; Khademhosseini, A.; Langer, R. Hydrogels in Biology and Medicine: From Molecular Principles to Bionanotechnology. *Adv. Mater.* **2006**, *18*, 1345–1360.
35. Consultancy, T. Fluorescein isothiocyanate dextran. *Prod. Inf.* 2010, 1–5.
36. Sigma Fluorescein Isothiocyanate-Dextran. *Prod. Inf.* 1997, 1–3.
37. Swift, J.; Ivanovska, I.L.; Buxboim, A.; Harada, T.; Dingal, P.C.D.P.; Pinter, J.; Pajerowski, J.D.; Spinler, K.R.; Shin, J.-W.; Tewari, M.; et al. Nuclear lamin-A scales with tissue stiffness and enhances matrix-directed differentiation. *Science* **2013**, *341*, 1240104.
38. Cai, Y.; Xu, C.; Chen, P.; Hu, J.; Hu, R.; Huang, M.; Bi, H. Development, validation, and application of a novel 7-day Caco-2 cell culture system. *J. Pharmacol. Toxicol. Methods* **2014**, *70*, 175–81.
39. Wells, R.G. The role of matrix stiffness in regulating cell behavior. *Hepatology*

2008, *47*, 1394–400.

40. Valls-Margarit, M.; Iglesias-García, O.; Di Guglielmo, C.; Sarlabous, L.; Tadevosyan, K.; Paoli, R.; Comelles, J.; Blanco-Almazán, D.,; Jiménez-Delgado, S.; Castillo-Fernández, O.; Samitier, J.; Jané, R.; Martínez, E.; Raya, A. Engineered Macroscale Cardiac Constructs Elicit Human Myocardial Tissue-like Functionality. *Stem Cell Reports* **2019**, *13*, 1–14.

41. Rodriguez-Boulan, E.; Kreitzer, G.; Müsch, A. Organization of vesicular trafficking in epithelia. *Nat. Rev. Mol. Cell Biol.* **2005**, *6*, 233–247.

42. Uroz, M.; Wistorf, S.; Serra-Picamal, X.; Conte, V.; Sales-Pardo, M.; Roca-Cusachs, P.; Guimerà, R.; Trepat, X. Regulation of cell cycle progression by cell-cell and cell-matrix forces. *Nat. Cell Biol.* **2018**, *20*, 646–654.

43. Sunyer, R.; Conte, V.; Escribano, J.; Elosegui-Artola, A.; Labernadie, A.; Valon, L.; Navajas, D.; García-Aznar, J.M.; Muñoz, J.J.; Roca-Cusachs, P.; et al. Collective cell durotaxis emerges from long-range intercellular force transmission. *Science* **2016**, *353*, 1157–61.

44. Rowart, P.; Erpicum, P.; Krzesinski, J.-M.; Sebbagh, M.; Jouret, F. Mesenchymal Stromal Cells Accelerate Epithelial Tight Junction Assembly via the AMP-Activated Protein Kinase Pathway, Independently of Liver Kinase B1. *Stem Cells Int.* **2017**, *2017*, 9717353.

45. Sung, J.H.; Yu, J.; Luo, D.; Shuler, M.L.; March, J.C. Microscale 3-D hydrogel scaffold for biomimetic gastrointestinal (GI) tract model. *Lab Chip* **2011**, *11*, 389–392.

46. Le Ferrec, E.; Chesne, C.; Artusson, P.; Brayden, D.; Fabre, G.; Gires, P.; Guillou, F.; Rousset, M.; Rubas, W.; Scarino, M.L. In vitro models of the intestinal barrier. The report and recommendations of ECVAM Workshop 46.

European Centre for the Validation of Alternative methods. *Altern. Lab. Anim.* **2001**, *29*, 649–68.

47. Göke, M.; Kanai, M.; Podolsky, D.K. Intestinal fibroblasts regulate intestinal epithelial cell proliferation via hepatocyte growth factor. *Am. J. Physiol.* **1998**, *274*, G809-18.

48. Haffen, K.; Simon-Assmann, P.; Kedinger, M.; Grenier, J.F.; Zweibaum, Z. [Permissive effects of human colonic cancer (HT-29 and Caco-2) on intestinal smooth muscle differentiation]. *C. R. Seances Acad. Sci. III.* **1981**, *293*, 807–12.

49. Wang, H.; Heilshorn, S.C. Adaptable hydrogel networks with reversible linkages for tissue engineering. *Adv. Mater.* **2015**, *27*, 3717–36.

50. Hynds, R.E.; Bonfanti, P.; Janes, S.M. Regenerating human epithelia with cultured stem cells: feeder cells, organoids and beyond. *EMBO Mol. Med.* **2018**, *10*, 139–150.

51. Visco, V.; Bava, F.A.; D'Alessandro, F.; Cavallini, M.; Ziparo, V.; Torrisi, M.R. Human colon fibroblasts induce differentiation and proliferation of intestinal epithelial cells through the direct paracrine action of keratinocyte growth factor. *J. Cell. Physiol.* **2009**, *220*, 204–13.

Figures and captions

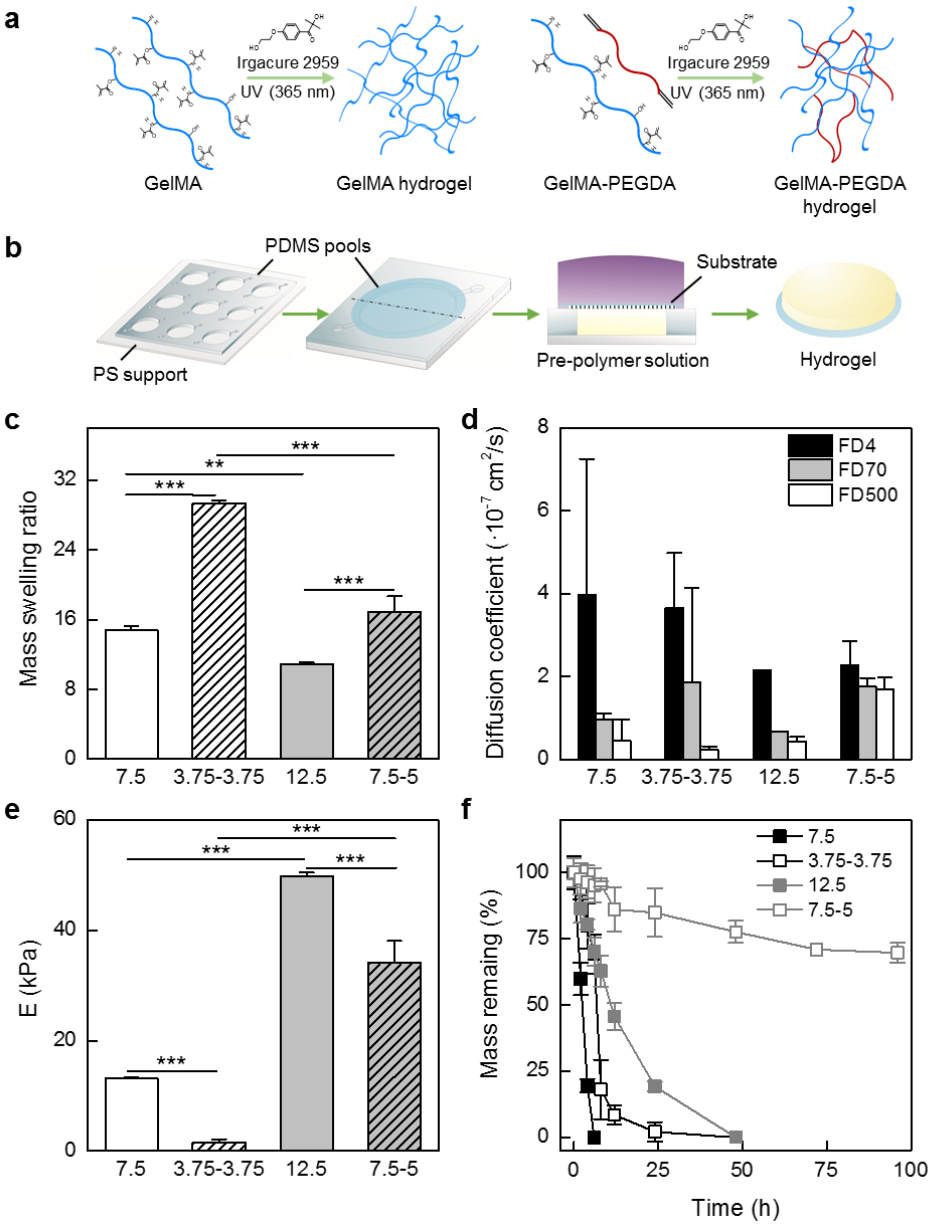

Figure 1. (a) Schematic of the GelMA and GelMA-PEGDA photo-polymerization reaction and co-networks formed. (b) Schematic of the single-step photo-crosslinking process employed. Pre-polymer solution was poured into a PDMS pool and covered with a cover glass or a porous membrane which both act as substrates. UV exposure produces either a single or an array of photo-crosslinked hydrogel networks. (c) Mass swelling ratio, (d) diffusion coefficient for different molecule sizes (FD500 = 500 kDa, with a hydrodynamic diameter of 32 nm; FD70 = 70 kDa, hydrodynamic diameter of 11.6 nm; FD4 4 kDa, hydrodynamic diameter of 2.8 nm), (e) bulk modulus, E, and (f) degradation

upon collagenase incubation (shown as mass remaining with time), for different GelMA networks and GelMA-PEGDA co-networks: 7.5 (7.5% w/v GelMA), 3.75-3.75 (3.75% w/v GelMA-3.75% w/v PEGDA), 12.5 (12.5% w/v GelMA), 7.5-5 (7.5% w/v GelMA-5% w/v PEGDA). Values are shown as mean ± SD (n=3). **p < 0.005 and ***p<0.001.

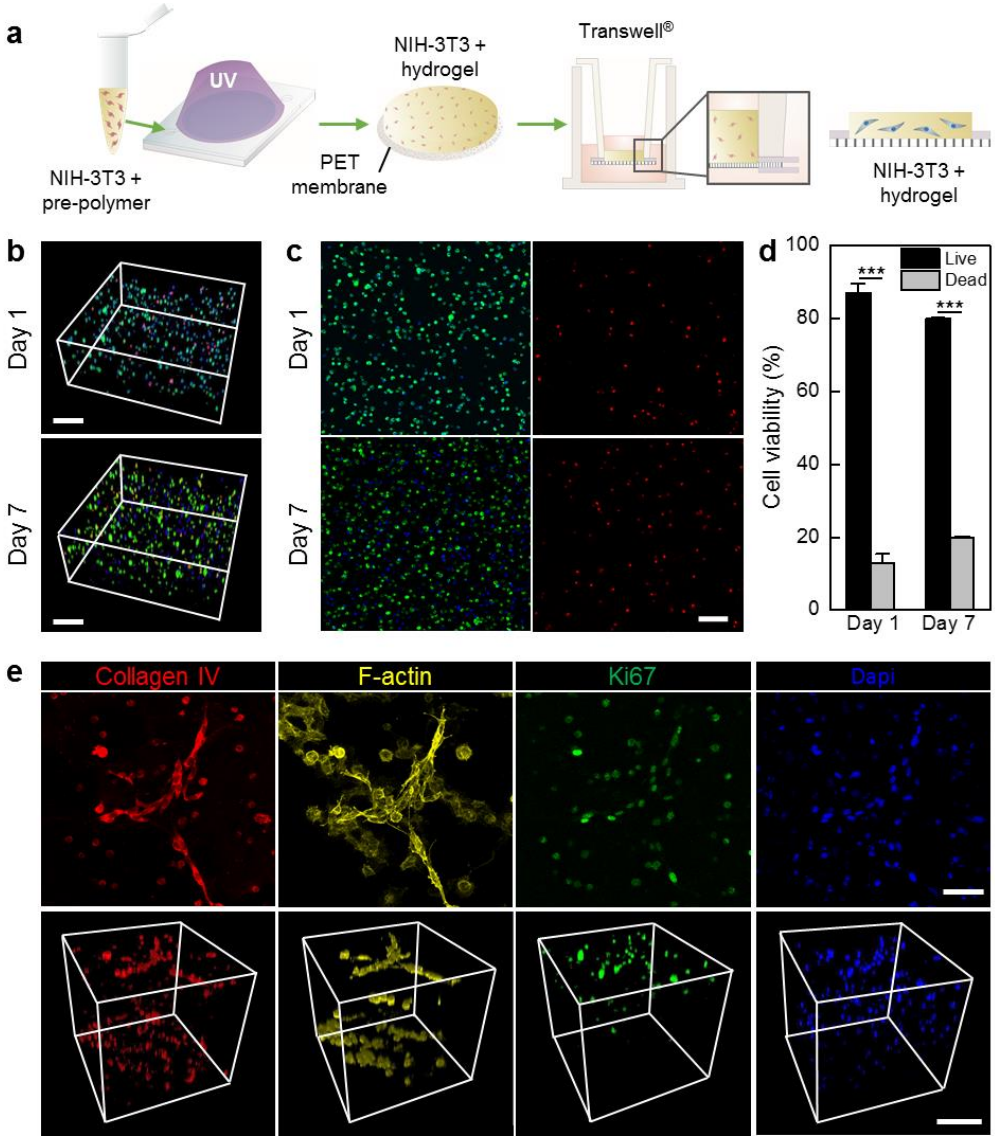

Figure 2. (a) Schematic to illustrate the NIH-3T3 fibroblast encapsulation process in the hydrogel co-network. (b) Confocal 3D reconstruction of the hydrogel co-network showing the spatial distribution of the NIH-3T3 embedded cells on days 1 and 7 after live/dead assays (live cells stain in green, dead cells in red). Dapi was used to stain the nuclei. Scale bars: 200 µm. (c) Maximum intensity projections of samples shown in panel

(b). Scale bar: 100 µm. (d) Quantification of cell viability at days 1 and 7 after encapsulation based on live/dead staining. Values are the mean percentage of cell viability ± SD (n=3), ***p<0.001. (e) Immunostaining for Collagen IV, F-actin, and Ki67 of hydrogel co-networks with embedded NIH-3T3 fibroblasts after 7 days in culture shown as maximum intensity projections (top panels) and confocal 3D reconstruction (bottom panels). Scale bars: 50 µm (top) and 100 µm (bottom panels).

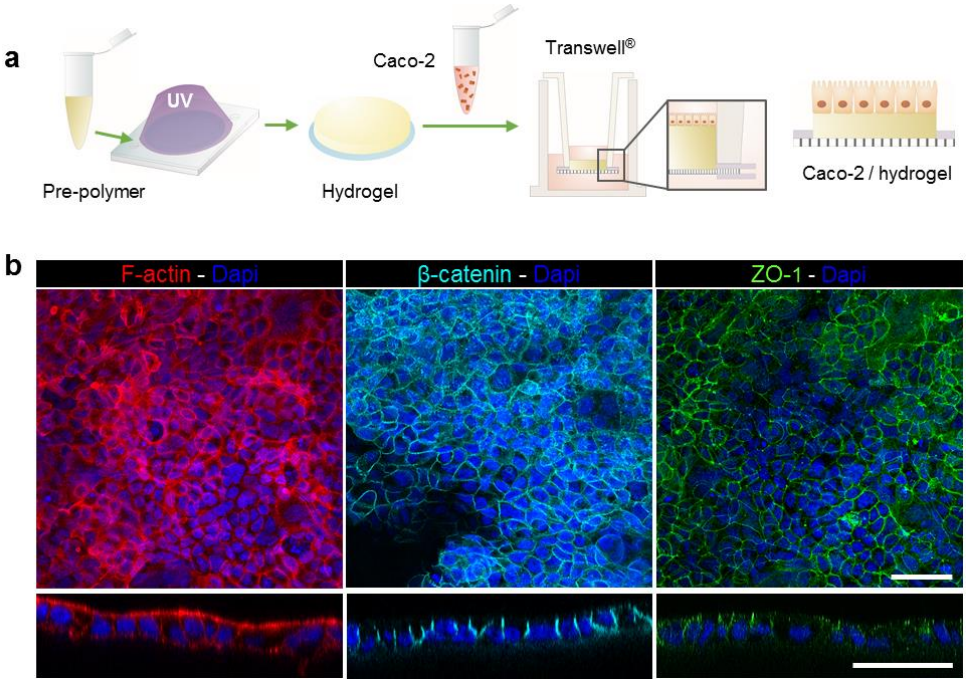

Figure 3. (a) Schematic to illustrate the Caco2 epithelial cells seeding method on the hydrogel co-network. (b) Maximum intensity projections of immunostainings for F-actin, β-catenin, and ZO-1 on the epithelial cell monolayer formed on top of the hydrogel co-networks (upper panels) and orthogonal sections (bottom panels). Dapi was used to stain the nuclei. Scale bars: 50 µm.

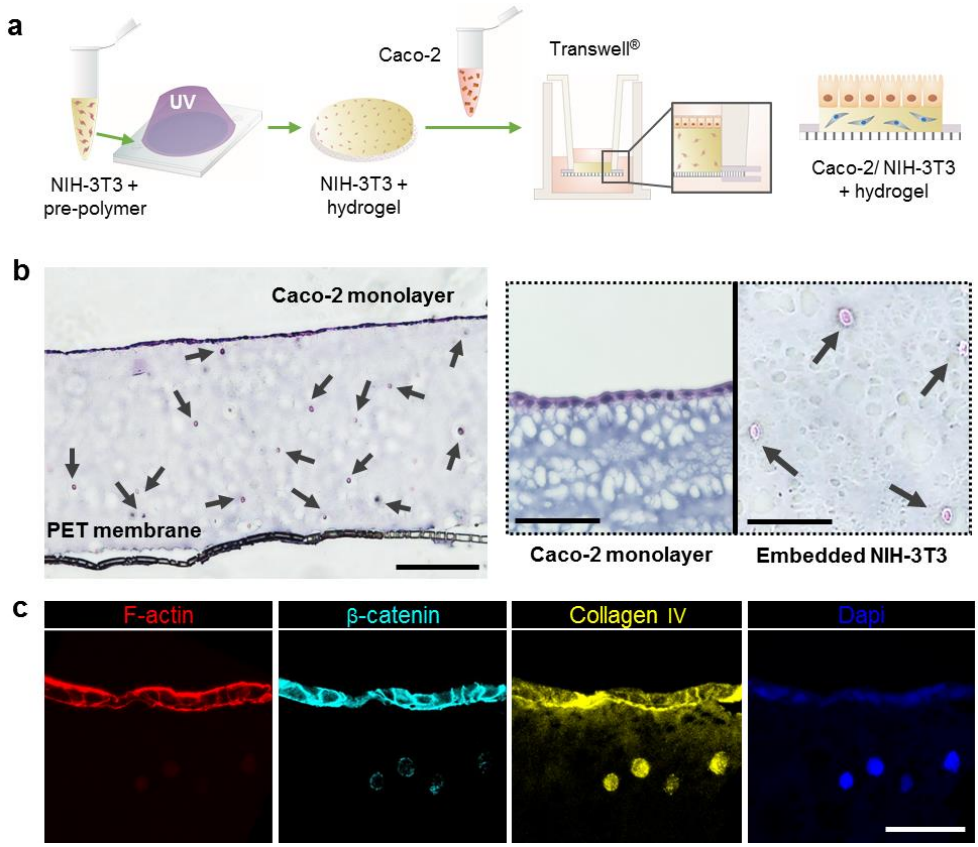

Figure 4. (a) Schematic to illustrate the NIH-3T3 fibroblast and Caco2 epithelial cell co-culture method in the hydrogel co-networks. (b) Cross-section of haematoxylin and eosin stained co-culture samples in hydrogel co-networks showing the formation of an intact epithelial monolayer at the top and a uniform distribution of the NIH-3T3 fibroblasts throughout the hydrogel (left panel). The right panel shows detailed views of both cell types. Scale bars: 150 µm (left) and 50 µm (right). (c) Immunostainings for F-actin, β-catenin, and Collagen IV of a co-culture sample in hydrogel co-networks. Scale bar: 50 µm. Dapi was used to stain the nuclei. All samples were fixed and stained after 21 days of culture.

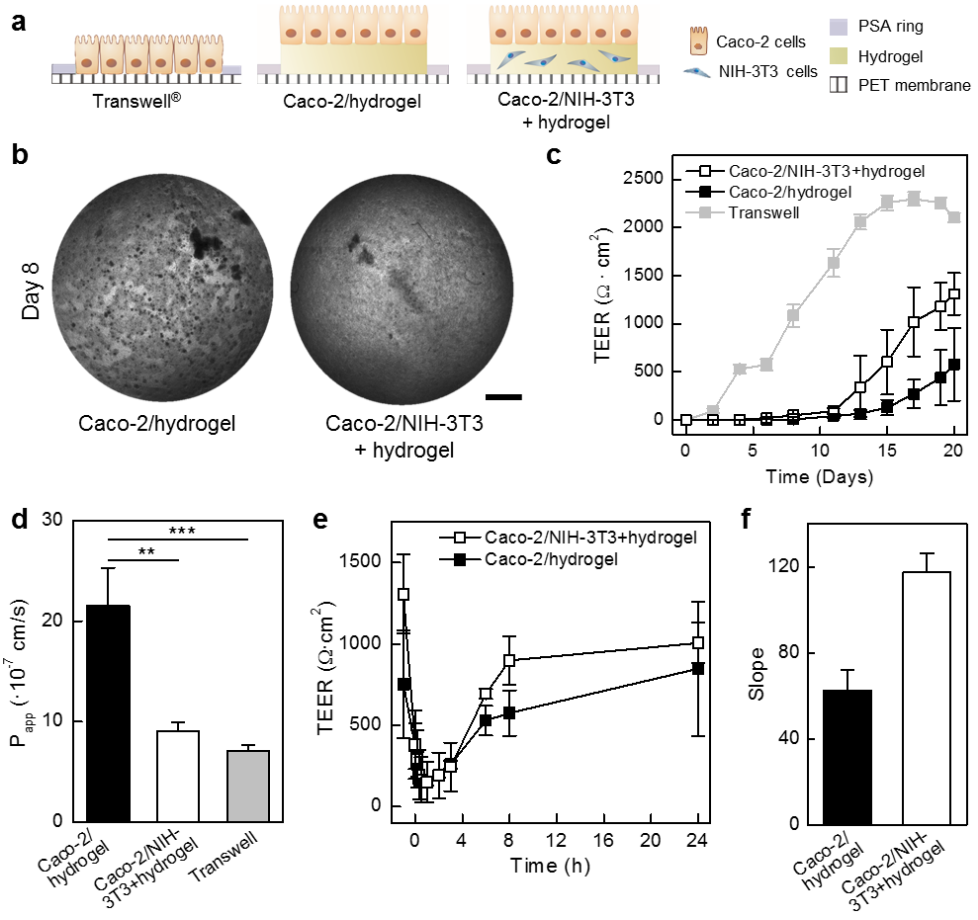

Figure 5. (a) Schematic illustration of the analysed cell culture configurations. (b) Bright field tile-scan images of the entire Transwell® membrane surface (0.33 cm^2) showing the epithelial monolayer growth on top of hydrogel co-networks with (right) and without (left) embedded NIH-3T3 cells after 8 days in culture. Scale bar: 1 mm. (c) Transepithelial electrical resistance (TEER) as function of cell culture time for epithelial monolayers grown on conventional Transwells® (grey) and on top of hydrogel co-networks with (white) and without (black) embedded NIH-3T3 fibroblasts. (d) Apparent permeability (P_{app}) of FITC-dextran 4 kDa (FDA) through epithelial monolayers grown on conventional Transwell® (grey) and on top of hydrogel co-networks with (white) and without (black) embedded NIH-3T3 fibroblasts. Values are mean ± SD (n=3). (e) TEER evolution upon EDTA treatment of the epithelial monolayer grown on hydrogel co-

networks in the presence or absence of embedded NIH-3T3. (f) Change of TEER over time from panel (e). Values are mean ± SD (n=3). **p < 0.005 and ***p<0.001.